CHEMISTRY

Efficient oral insulin delivery enabled by transferrin-coated acid-resistant metal-organic framework nanoparticles

Jun-Jie Zou[1], Gaohui Wei[1], Chuxiao Xiong[1], Yunhao Yu[1], Sihui Li[1], Liefeng Hu[1], Shengqian Ma[2]*, Jian Tian[1]*

Oral protein delivery is considered a cutting-edge technology to improve patients' quality of life, offering superior patient compliance and convenience compared with injections. However, oral protein formulation has stagnated because of the instability and inefficient penetration of protein in the gastrointestinal tract. Here, we used acid-resistant metal-organic framework nanoparticles (UiO-68-NH_2) to encapsulate sufficient insulin and decorated the exterior with targeting proteins (transferrin) to realize highly efficient oral insulin delivery. The UiO-68-NH_2 nanocarrier with proper pore size achieved high insulin loading while protecting insulin from acid and enzymatic degradation. Through receptor-mediated transcellular pathway, the transferrin-coated nanoparticles realized efficient transport across the intestinal epithelium and controlled insulin release under physiological conditions, leading to a notable hypoglycemic effect and a high oral bioavailability of 29.6%. Our work demonstrates that functional metal-organic framework nanoparticles can protect proteins from the gastric environment and overcome the intestinal barrier, thus providing the possibility for oral biomacromolecule delivery.

INTRODUCTION

Diabetes is a chronic metabolic disease that affects more than 470 million people around the world (*1*). Because of its high prevalence, disability, and fatality rate, diabetes has become a serious global health problem (*2*, *3*). The treatment of type 1 diabetes or advanced type 2 diabetes relies on routinely subcutaneous insulin (INS) injections. Still, long-term INS subcutaneous injections are accompanied by various side effects, resulting in poor patient compliance (*4*–*6*). Hence, the development of noninvasive INS delivery methods is in urgent need. Among various noninvasive methods of administration, oral administration has been the most widely used way because of its painlessness and convenience (*7*–*9*). Nevertheless, barely any protein pharmaceutical preparations have been approved for oral administration in clinic practice, primarily because of the formidable physiological barrier in the gastrointestinal (GI) tract (*10*). These barriers mainly include harsh acids and proteases in the stomach, the impermeable mucus layer, and the tightly connected intestinal epithelial cell layer in the intestine, which severely hampered the absorption efficiency of active protein formulations (*11*, *12*). Above all, how to maintain high protein activity and allow proteins to penetrate through the epithelial cell layer into the bloodstream are considered the main challenges of any oral drug formulation.

To overcome the above-mentioned absorption barriers, scientists have developed numerous nanoparticle (NP) platforms for oral protein delivery, such as liposomes, polymeric NPs, and silica NPs (*13*–*18*). However, the capability of these NPs for practical protein delivery applications still remains limited, suffering from inefficient protein loading and protection, low intestinal permeation, uncontrollable release, or complicated formulation strategies. In recent years, using enteric materials and penetration enhancers has received substantial attention to enhance the efficacy of protein delivery (*19*–*22*). However, enteric coating involves additional excipients and formulation steps. Penetration enhancers are associated with a risk of destroying the tight junctions of the intestinal epithelial cell layer, which may lead to bacterial infection (*23*, *24*). Therefore, it is vital to achieve effective protein absorption without destroying the tight junctions of the intestinal epithelial cell layer. From this perspective, some progress has been made in the design of macromolecular protein drug carriers using various specific receptors highly expressed on the intestinal epithelial cell membrane, such as transferrin receptors (TfR) and FcRn receptors (*25*–*27*). For instance, transferrin (Tf) widely exists in the human body, which guides iron absorption and transportation by binding to TfR on epithelial cells (*28*, *29*). Notably, studies on Tf/TfR-mediated targeted protein delivery systems produced exciting results in cancer, central nervous system diseases, and oral administration (*30*–*32*). Peppas and co-workers (*33*) reported that the Tf-INS conjugate increased the permeability of INS across the epithelial barrier by receptor-mediated transcytosis. Nevertheless, the fate of Tf in cells after transcytosis is going to lysosomes (*31*, *34*), where the abundant proteases could damage protein structure (*35*, *36*), leading to limited bioavailability. Farokhzad and co-workers (*29*) developed Tf-coated polymeric NPs for oral INS delivery, in which the surface-loaded Tf could enhance their transepithelial transport via receptor-mediated transcytosis. However, these NPs demonstrated unfavorable INS release before the transepithelial transport that restricted their pharmacological availability (~7.8%). Therefore, the development of functional nanosystems to protect the protein from the harsh gastric environment while improving the penetration efficacy through the intestine and realizing controlled release is of great significance for oral protein delivery.

Among numerous nanomaterials, nanoscale metal-organic frameworks (nMOFs) have emerged as promising candidates for drug delivery (*37*–*40*). nMOFs are a relatively new class of hybrid porous materials composed of metal ions or clusters bridged by organic ligands, which have ordered pore structure, large specific surface area, and abundant modification sites (*41*). Therefore, nMOFs hold

[1]Key Laboratory of Combinatorial Biosynthesis and Drug Discovery (MOE), School of Pharmaceutical Sciences, Wuhan University, Wuhan 430071 P. R. China. [2]Department of Chemistry, University of North Texas, Denton, TX 76201, USA.
*Corresponding author. Email: shengqian.ma@unt.edu (S.M.); jian.tian@whu.edu.cn (J.T.)

great potential as drug transport carriers since they can achieve extremely high drug loading capacity (LC) and connect with different molecules as needed to fulfill various functions (*42*–*44*). Moreover, the reversible coordination between ligands and metal ions inside endow the nMOFs with the characteristics of controlled releasing, biodegradability, low toxicity, and good biocompatibility (*45*). Recently, Farha and co-workers (*46*) reported a mesoporous Zr-based MOF (NU-1000) as an INS carrier, protecting INS from simulated harsh stomach environments and controlling INS release under physiological conditions. Although the preliminary in vitro release test achieved favorable results, the problem of low protein permeability in the intestinal epithelial cell layer remained to be solved, and there was still a lack of in vivo study evidence to prove whether effective INS absorption can be achieved. To the best of our knowledge, no research about MOF-based nanosystems protecting INS from a harsh environment while improving the INS penetration efficacy has been reported to achieve a superior hypoglycemic effect ultimately.

Here, using acid-resistant nMOFs (UiO-68-NH_2) with exterior targeting protein (Tf) decoration, we elaborately constructed a nanosystem with protein protection and intestinal transportation functions for the highly efficient oral INS administration. The selection of the UiO-68-NH_2 NPs was primarily based on their sufficient porosity, acid stability, and phosphate ion instability. The ligand molecule of UiO-68-NH_2 is longer than that of most MOFs being reported (*47*), leading to a larger pore structure with a diameter of ~2.6 nm (*48*) to load sufficient INS (~2 nm in monomeric form) but exclude pepsin (~6 nm) (*46*). This steric hindrance effect between UiO-68-NH_2 and macromolecule proteases could protect INS from proteolysis in the GI tract. The acid stability and phosphate ion instability of UiO-68-NH_2 could protect INS well in harsh acidic environments and realize controllable INS release under phosphate-rich physiological conditions. As for the targeting protein, Tf meets the critical requirements of the targeting agent for oral administration: (i) Intestinal epithelial cells express a large number of receptors for Tf to combine (*49*), and (ii) Tf has good stability in the GI tract as well because of the ability to partially resist the degradation of trypsin and chymotrypsin (*32*). Consequently, in this study, we loaded INS into highly porous UiO-68-NH_2 NPs (denoted as I@U) and further coated the exterior side with Tf on (T@I@U), as illustrated in Fig. 1. The encapsulated INS within the UiO-68-NH_2 NPs could be well protected from the gastric environment including harsh acid and protease, and exhibited controlled release in physiological conditions. Moreover, the Tf-coated acid-resistant MOFs oral delivery nanosystem can be rapidly absorbed by intestinal cells and escape from lysosomes for deeper penetration, which is adequate for rapid and efficient intestinal transportation and ultimately achieving a favorable therapeutic effect. In addition, the preparation of such a nanosystem, based on a single-step solvothermal reaction from readily available starting materials, is simple, low cost, and easily scale-up. This research represented a proof of concept of using the targeting protein-coated acid-resistant nMOFs for oral INS administration, displaying the great potential of efficient oral protein delivery.

RESULTS

Preparation and characterization of nMOF-based protein delivery nanosystems

The preparation procedures for UiO-68-NH_2 NPs, I@U NPs, and T@I@U NPs are shown in Fig. 1. UiO-68-NH_2 NPs with uniform regular octahedron shapes were obtained through the facile one-step solvothermal method. The changes in morphology and particle size of NPs were negligible after loading the INS. The hydrodynamic diameters of UiO-68-NH_2 and I@U were 156.4 ± 1.9 and 157.7 ± 0.2 nm, respectively, and the angles of the regular octahedron were relatively sharp. When varying amounts of Tf were decorated on the surface via physical adhesion, the angles of NPs gradually became blunt (fig. S1). The morphology of NPs after Tf coating gradually changed from a regular octahedron to a sphere, and the size increased to 171.7 ± 3.4 nm. The zeta potentials of UiO-68-NH_2 NPs rose from +25 to +35 mV after loading with INS and nearly approached +40 mV after further decoration with Tf (Fig. 2, A and B). The successful immobilization of rhodamine B isothiocyanate (RITC)–labeled INS in UiO-68-NH_2 NPs was confirmed by ultraviolet-visible (UV-vis) spectroscopy, in which the maximum absorption of RITC slightly redshift from 558 nm of free RITC-INS solution to 567 nm of the encapsulated form (fig. S2). The confocal laser scanning microscopy (CLSM) and optical images further indicated that RITC-labeled INS was distributed throughout the UiO-68-NH_2 crystals (fig. S3). Owing to the positively charged nature of UiO-68-NH_2 NPs and INS at the acidic condition (pH 4) of the loading process (fig. S4), the INS encapsulation was mainly driven by hydrophobic interactions between the hydrophobic surface of UiO-68-NH_2 and INS instead of electrostatic interactions. In addition, fluorescein isothiocyanate (FITC)–labeled Tf and RITC-labeled INS were used in preparing the dual-fluorescence–labeled nMOFs to prove the formation and the structural integrity of T@I@U. FITC and RITC are commonly used as fluorescence resonance energy transfer (FRET) fluorescence pairs. FRET phenomenon would occur when the distance between FITC and RITC is less than 10 nm (*50*). Figure 2C exhibited the fluorescence spectra where a strong FRET signal could be observed. The emission intensity of FITC-Tf decreased sharply at 520 nm, while that of RITC-INS significantly increased at 585 nm, clarifying the coexistence and spatial proximity of INS and Tf in T@I@U NPs. The powder x-ray diffraction (PXRD) patterns of both I@U and T@I@U NPs were essentially the same as that of UiO-68-NH_2 NPs and the calculated pattern from UiO-68-NH_2 single crystals (Fig. 2D), which demonstrated that UiO-68-NH_2 maintained its crystallinity throughout the encapsulation and decoration process. In addition, the energy-dispersive spectroscopy (EDS) elemental mapping analyses were tested to confirm the existence of each component in T@I@U NPs (S for proteins, Fe for Tf, and Zr for UiO-68-NH_2). As shown in Fig. 2E, the elements of S, Zr, and Fe were uniformly distributed on the NPs, and the range of S was significantly more extensive than that of Zr, which provided direct evidence for the successful fabrication of T@I@U. Consequently, it can be concluded that the macromolecules of INS were loaded into UiO-68-NH_2 successfully with Tf uniformly decorated on the I@U NPs. The INS-loading behaviors of UiO-68-NH_2 NPs were further explored using the bicinchoninic acid (BCA) method by simply mixing INS and UiO-68-NH_2 NPs at a mass ratio from 1:1 to 6:1 (fig. S5). The UiO-68-NH_2 NPs exhibited a high LC of 33 weight % (wt %) at the feeding ratio of 4:1, higher than most of the INS nanocarriers being reported (table S1) (*29*, *51*). The mass loss was also observed to determine the LC of the UiO-68-NH_2–based nanosystem by thermogravimetric analysis (TGA), which was consistent with the above results (fig. S6). The high LC and facile exterior modification of UiO-68-NH_2 make it an ideal candidate for INS nanocarrier.

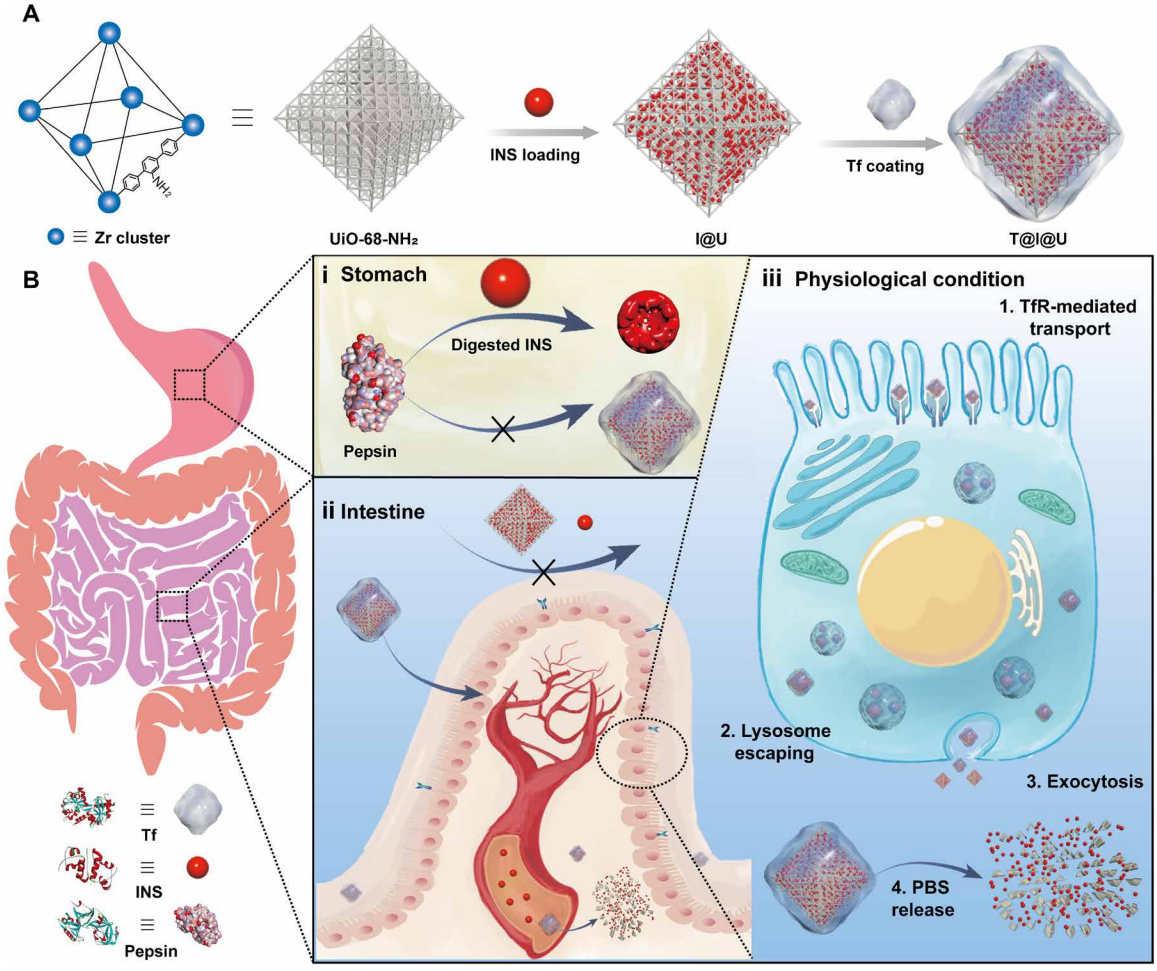

Fig. 1. Schematic representation of Tf-coated acid-resistant nMOF nanosystem for oral delivery of INS. (**A**) The synthesis of the UiO-68-NH_2–based nanosystems. (**B**) The oral delivery process of the Tf-coated UiO-68-NH_2 nanosystem in vivo addresses both the harsh environment in the stomach (i) and the epithelial cell layer barriers (ii). (iii) The Tf-coated UiO-68-NH_2 nanosystem contributed to overall intensive intestinal cell absorption under physiological conditions.

In vitro stability and protein protection performance of Tf-coated nMOFs

To evaluate the in vitro stability of the UiO-68-NH_2–based nanosystems, we monitored the changes in size and morphology under various situations at different time intervals. No noticeable change in particle size was observed when different formulations were dispersed in a simulated gastric pH environment (dilute HCl, pH 2) for 14 days, owing to the strong acid-proof stability of the UiO-68-NH_2 (Fig. 3A). In contrast, the particle size of I@U increased significantly under the physiological condition because the UiO-68-NH_2 began to clump together and disintegrate (figs. S7 and S8). After being coated with Tf, the deconstruction was greatly retarded, demonstrating that Tf decoration endowed the nanosystem with slow-release performance in physiological conditions.

We next explored the ability of UiO-68-NH_2 in protecting INS against protease degradation. As shown in Fig. 3B, free INS was almost completely degraded after only 1 hour in the trypsin-containing Hanks' balanced salt solution (HBSS) buffer, while about 80% of active INS remained in the I@U group. The result demonstrated that INS was protected from degradation because of a certain steric hindrance between INS and the protease after being encapsulated in UiO-68-NH_2. In addition, the residual amount of INS was higher than 50% after 2 hours because of the protective effect of Tf, as mentioned above. Together, the protection effect of Tf-coated acid-resistant nMOFs provided a favorable prerequisite for the long-term circulation of nanosystems in vivo.

Sustained and controlled INS release kinetics of T@I@U

As an effective oral delivery nanocarrier, UiO-68-NH_2 has proven its adequate protection for INS against severe conditions. Meanwhile, the steady release of INS from the acid-resistant nMOFs in physiological conditions was also demanded. The release profiles of INS from I@U and T@I@U under simulated GI environment (FaSSGF for simulated gastric fluid and FaSSIF without phosphate for simulated intestine fluid) and simulated physiological conditions [phosphate-buffered saline (PBS), pH 7.4] are shown in Fig. 3C. Under the FaSSGF, FaSSIF, and double distilled H_2O (ddH_2O) environment (fig. S9), less than 20% of INS from I@U and T@I@U were released in 24 hours. While under the PBS condition, INS was slowly released from UiO-68-NH_2, and the cumulative released INS from I@U and T@I@U reached 99.1 and 90.3% at 12 hours, respectively. Continuous release of INS under different environments was

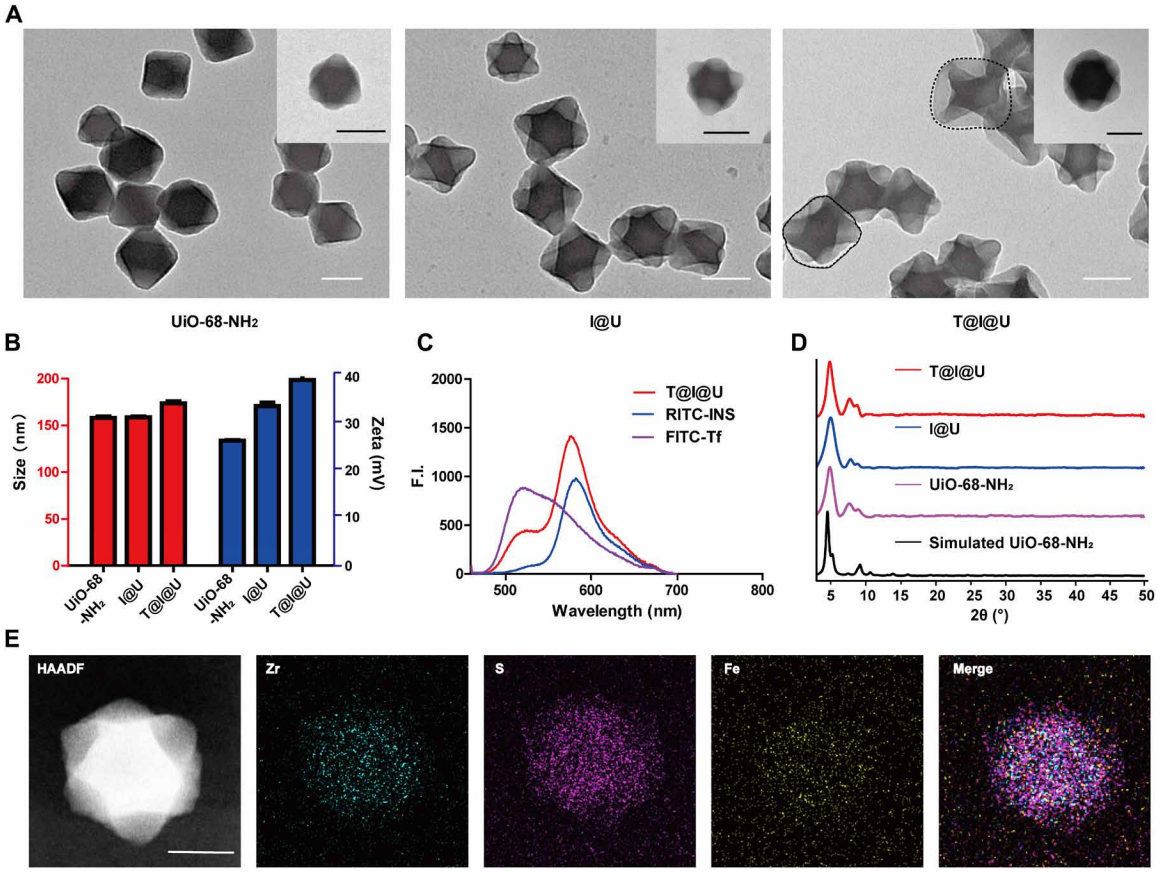

Fig. 2. Characterization of UiO-68-NH_2, I@U, and T@I@U. (**A**) The TEM images of UiO-68-NH_2–based nanosystems. Scale bars, 100 nm. (**B**) The hydrodynamic size and zeta potential of different preparations measured by DLS using the NPs dispersion in ddH_2O. (**C**) Emission spectra of different preparations with excitation at 450 nm. F.I., fluorescence intensity. (**D**) The PXRD profile of UiO-68-NH_2, simulated UiO-68-NH_2, I@U, and T@I@U. (**E**) The EDS elemental mapping analyses of T@I@U. Scale bar, 50 nm.

also evaluated to simulate the status of orally taken drugs (Fig. 3D). Barely any INS was released from neither I@U nor T@I@U under acidic to neutral pH conditions in the stomach and intestine. However, after being incubated in a neutral PBS environment, I@U and T@I@U started to deconstruct and release INS. The INS from I@U was almost completely released within 10 hours in PBS, while the percent of released INS from T@I@U was only about 80%. Consistent with the stability result, Tf slightly hindered the disintegration of UiO-68-NH_2 and slowed down the release rate of INS. The above results indicated that the release of INS from Tf-coated nMOFs had considerable environmental sensitivity, which was specifically triggered by phosphate in PBS rather than pH. In general, T@I@U exhibited sustained and controlled release kinetics.

To further verify that the activity of INS was not destroyed during the entire experiment, we examined the bioactivity of INS after the drug release process by subcutaneously injecting free INS and INS released from PBS-treated I@U and T@I@U into diabetic rats. As depicted in Fig. 3E, the released INS from I@U and T@I@U produced a notable hypoglycemic effect analogous to an equivalent dose of free INS solution, indicating that the process of INS immobilization in UiO-68-NH_2 did not impair its activity, which was essential for the subsequent experiments.

Biocompatibility and long-term safety analysis

We further examined the biocompatibility of the UiO-68-NH_2–based nanosystems through in vitro cell viability and live/dead imaging. As shown in fig. S10, all samples exhibited negligible cytotoxicity (cell viability >85%) on three different cell lines even when the concentration reached 500 μg/ml, which was also confirmed through live/dead staining. To examine potential cell membrane disruption, T@I@U was incubated with erythrocytes for 4 hours, and there was no evidence of hemolysis. The hemolysis rate was 3.23% when the concentration reached 1 mg/ml, verifying that T@I@U barely caused damage to cell membranes. Meanwhile, no obvious reduction of transepithelial electrical resistance (TEER) was observed when the cell monolayer was exposed to I@U and T@I@U (Fig. 3F), which confirmed the integrity of the tight junctions. Inspired by the low toxicity of single-dose T@I@U, we further examined the potential long-term toxicity of the UiO-68-NH_2–based nanosystem via an extended in vivo experiment. As illustrated in fig. S11, the finger-like villi were observed in the small intestine tissue of mice, indicating the intact structure of the intestine after twice-daily T@I@U treatment for seven consecutive days. In addition, no apparent structural damage occurred to the organs and small intestine tissue. The above results corroborated the good biocompatibility of the UiO-68-NH_2–based nanosystem.

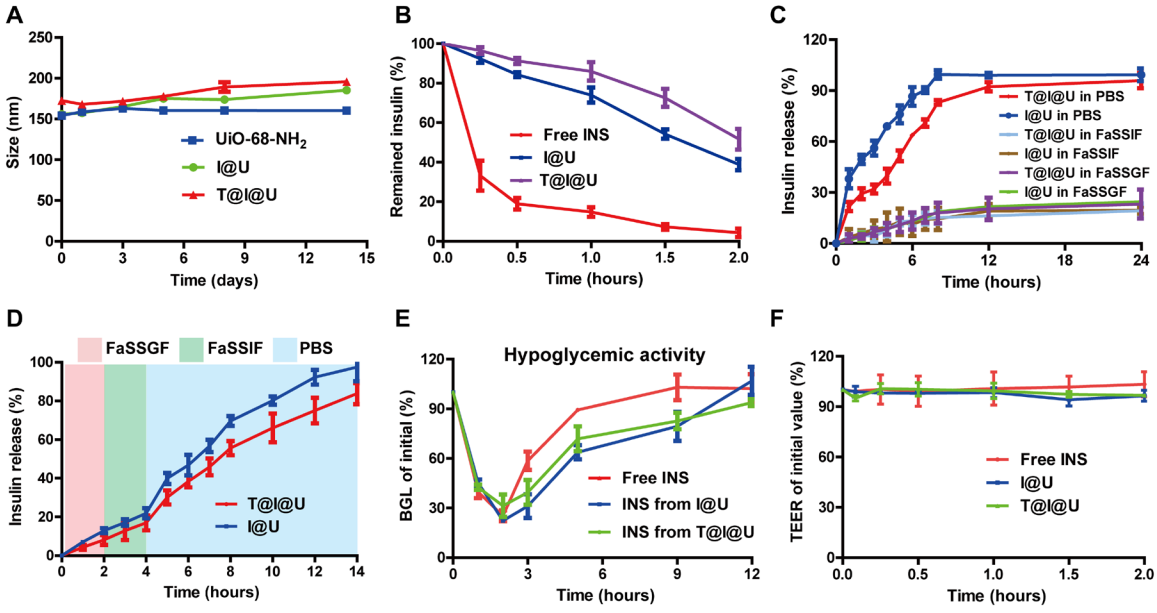

Fig. 3. The in vitro release and penetration performance of the Tf-coated UiO-68-NH_2 nanosystem. (**A**) The size stability of UiO-68-NH_2–based nanosystems in ddH_2O (pH 2) incubated at 4°C for 14 days. (**B**) The enzymatic degradation profiles from different preparations after being incubated with trypsin in HBSS buffer at 37°C for various time points ($n = 3$ independent samples, means ± SD). (**C**) The in vitro release kinetics of I@U and T@I@U in different conditions ($n = 3$ independent samples, means ± SD). (**D**) Continuous release of INS from I@U and T@I@U under different environments ($n = 3$ independent samples, means ± SD). (**E**) Blood glucose response of normal rats to free INS and INS released from the UiO-68-NH_2–based nanosystems ($n = 3$ biologically independent animals, means ± SD). (**F**) Effects of different formulations on TEER of Caco-2 cell monolayers ($n = 3$ biologically independent samples, means ± SD).

Tf-mediated enhanced cellular internalization and transepithelial activity of T@I@U

Similar to the structure and function of small intestinal epithelial cells, human colon adenocarcinoma (Caco-2) cells were currently used to study the transportability of drugs across the intestinal barrier to predict drug absorption. This research used Caco-2 cells as an in vitro model and learned whether Tf-coated nMOFs could traverse the intestinal epithelium by TfR-mediated endocytosis and successfully escape the lysosome for deeper penetration (Fig. 4A). We determined the qualitative and quantitative uptake of the above-mentioned fluorescence-labeled UiO-68-NH_2–based NPs by Caco-2 cell monolayers. Since INS is a biological macromolecule with high polarity and strong hydrophilicity, INS has poor passive diffusion and transmembrane ability. Only a small amount of fluorescence was observed in the free INS and I@U groups in Fig. 4B as expected, while the Tf-coated nMOFs exhibited a much stronger fluorescence signal compared with the other groups. The results demonstrated a TfR-mediated better uptake effect, which was further confirmed by the deeper fluorescence distribution along the *z* axis and the flow cytometry analysis. The quantitative cellular uptake level of T@I@U was approximately 2.25 times that of free INS and 1.5 times that of I@U groups (Fig. 4C). TfR-mediated cell internalization was time dependent, and the cell uptake level was as high as 53.2% in only 30 min, indicating the rapid and effective internalization of Tf-coated nMOFs (Fig. 4D).

As mentioned above, Tf-coated nanocarriers undergo transcytosis by binding to TfR on epithelial cell membranes. Therefore, to confirm the fate of Tf-coated nMOFs during the transport process, we explored the distribution of dual-fluorescence–labeled nMOFs in Caco-2 cell monolayers. After using T@I@U to incubate the cells for only 5 min, the green fluorescence of Tf was distributed around the cell, which indicated that it could rapidly bind to the receptor on the cell membrane. After 30 min of incubation, the fluorescence location results demonstrated that Tf had quickly and effectively transferred the nMOFs into the cell monolayers (Fig. 4E). In addition, we preincubated the cell monolayer with an excessive amount of free Tf as the competitive inhibitor. The free Tf would preferentially bind with the TfR on the apical side, while the cellular uptake level of T@I@U dropped significantly to 62% (Fig. 4F). The above results demonstrated that the uptake of T@I@U mainly occurred through TfR-mediated active endocytosis.

After endocytosis, the nMOFs would be transported to the lysosome for digestion. Although, as demonstrated above, nMOFs could partially protect INS from being degraded by proteases, INS would gradually become inactive if it failed to escape the lysosome. Therefore, we explored the behavior of Tf-coated nMOFs when interacting with lysosomes via CLSM. Mechanically, the Tf-coated acid-resistant nMOFs had a strong positive charge and a unique membrane switching effect through electrostatic interaction with the lysosome membrane, leading to lysosome escape. As shown in Fig. 4G and fig. S12, after just 15 min of incubation, almost all fluorescence signal of T@I@U was trapped within the lysosome, confirming that nMOFs can be quickly internalized through the TfR-mediated pathway. As the incubation time prolonged to 2 hours, the colocalization of the T@I@U and lysosome was reduced sharply (Fig. 4H), further indicating an effective escape from the inner lysosome compartment to avoid INS degradation. We observed that the colocalization rate slightly increased at 4 hours of incubation, implying that the escaped nMOFs might be reinternalized by the cells without removing the incubation media. We subsequently detected the INS degradation rate of different formulations in the Caco-2 cell monolayers. As shown in fig. S13, about 50% of

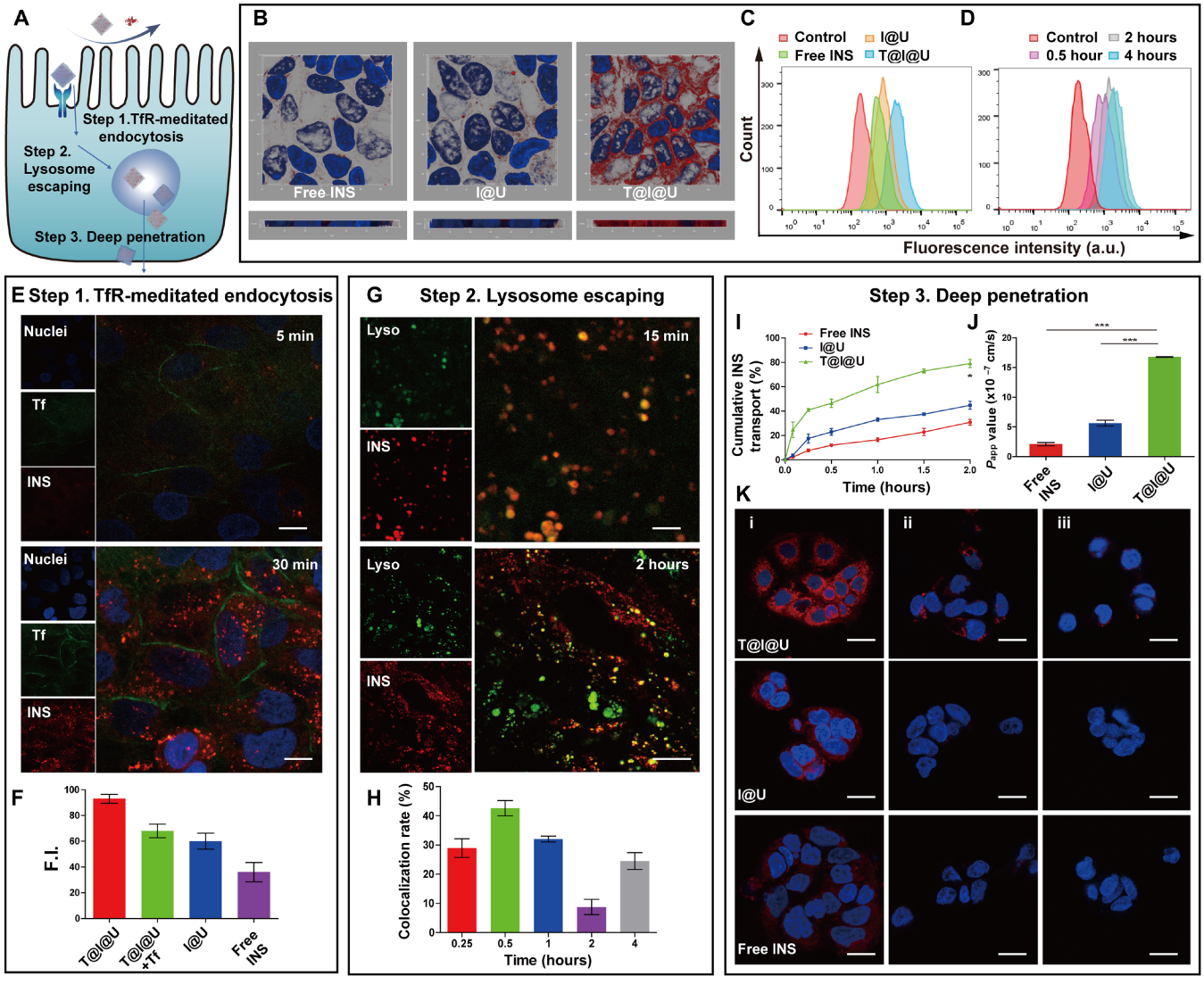

Fig. 4. TfR-mediated apical endocytosis of T@I@U. (**A**) Schematic illustration of transepithelial transport of INS from T@I@U to overcome multiple barriers of the intestinal epithelium by TfR-mediated pathway. (**B**) CLSM three-dimensional images of Caco-2 cell monolayers incubated with RITC-labeled free INS, I@U, and T@I@U for 2 hours (blue for nuclei and red for INS). Quantitative determination of cellular uptake amounts for different treatments at 4 hours (**C**) and T@I@U at various time points (**D**). (**E**) Distribution of Tf (green) and INS (red) after the cellular treatment at different time points. Scale bars, 10 μm. (**F**) Quantitative determination of cellular uptake amounts for different treatments at 2 hours ($n = 3$ biologically independent samples, means ± SD). CLSM graphs of lysosomal escape of T@I@U (**G**) and quantitative colocalization analysis of lysosome at different time points (**H**). Scale bars, 5 μm. The (**I**) cumulative transportation and (**J**) apparent permeability coefficient (Papp) of INS from different formulations across Caco-2 cell monolayer in 2 hours ($n = 3$ biologically independent samples, means ± SD). ***$P < 0.001$. (**K**) Intracellular transfer of different INS formulations visualized by CLSM ($n = 3$ biologically independent samples, means ± SD). Caco-2 cells on coverslips (i) were cultured in a medium that contained different INS formulations for 4 hours. Then, coverslip (i) was put into fresh culture medium and fresh cells on the coverslip (ii) for 12 hours. The above step was repeated to obtain the coverslip (iii). Scale bars, 25 μm. a.u., arbitrary units.

ingested INS in the free INS group was degraded after 2 hours of incubation, while the I@U and T@I@U groups significantly inhibited the degradation rate of INS. Only about 25% and less than 10% of INS were degraded, attributed to the protection of the UiO-68-NH_2 and the ability of T@I@U to escape the lysosome.

At length, the basolateral membrane was the last barrier hindering the transport of INS into the bloodstream circulation. Hence, we evaluated the transcellular transportation through the basolateral side of different preparations. First, we analyzed the transepithelial permeability of INS from different formulations across the Caco-2 cell monolayer. In just 5 min, the INS transport through the cell monolayer in the T@I@U group had exceeded 20%. The cumulative penetration INS reached 80% after 2 hours, far exceeding the free INS and I@U groups. Meanwhile, the apparent permeability coefficient (Papp) is an essential parameter for investigating the permeability of drugs. After careful calculation, the Papp of T@I@U was 16.8×10^{-7} cm/s, 8.05- and 2.98-fold higher than that of free INS and I@U, respectively (Fig. 4, I and J). The apparent changes of Papp indicated that Tf has significantly increased the penetration of INS through the cell monolayer, indicating that the nanosystem has

entered into the cell in large quantities and successfully exocytosed from the basal side. Moreover, the transcellular transport of T@I@U was further evaluated by the protocol previously reported in the literature (*52*). As shown in Fig. 4K, the INS signal of I@U and free INS groups had limited transportation among different batches of cells. In contrast, the fluorescence signal from T@I@U was high on coverslips (ii) and (iii). This phenomenon demonstrated that the INS took up on coverslip (i) was exocytosed into the medium and subsequently internalized by the cells on coverslips (ii) and (iii), which made it conducive to drug penetration through the intestine. Overall, the apical endocytosis markedly increased via the TfR-mediated uptake pathway, and the protection of MOF reduced the degradation of INS in the lysosome. Hence, the permeability of INS across Caco-2 cell monolayers was significantly improved upon Tf-coated acid-resistant MOFs.

Improved penetration efficiency of T@I@U in the isolated small intestine

Since the intestinal epithelium layer has been considered the most challenging barrier to the oral absorption of nanocarriers, this research further validated the ability of T@I@U to transport across the small intestinal ex vivo after the Tf-coated nMOFs were found to be effective at the cellular level in previous in vitro experiments. We compared the transport of free INS, I@U, and T@I@U across the intestinal epithelium in the duodenum, jejunum, and ileum loops. As shown in Fig. 5 (A to C), the INS permeation amounts of different preparations were all time dependent, especially the T@I@U group. Compared with the free INS and I@U NP groups, the T@I@U exhibited the highest accumulative amounts of INS permeated through each small intestinal section. At 2 hours, the infiltration amount of INS from the T@I@U group in the duodenum was approximately 127 mIU. Moreover, we found a gradual decrease in INS penetration from the duodenum to the jejunum to the ileum as well, probably due to a gradual reduction of TfR and a gradual increase in mucus throughout the small intestine. The above results illustrated that the absorption of T@I@U in the small intestine was dependent on the Tf-targeted pathway, which corresponded with the results obtained in cellular studies.

In vivo biodistribution and intestine absorption

The in vivo intestinal absorption and distribution of INS were further determined by Maestro in vivo imaging system and CLSM. The in vivo images showed the fluorescence signal and intensity distribution of RITC-INS from three different formulations within 24 hours (Fig. 5D). After 4 hours postadministration, a strong fluorescence signal was observed in the mice treated with T@I@U, which was greater than those in the free INS and I@U groups. The strong fluorescence of the mice treated with T@I@U reached the maximum at 8 hours, and this phenomenon persevered for 12 hours, which provided solid evidence for the long-term effect of the T@I@U NPs.

The biodistribution of INS fluorescence was also observed in intestines and major organs after 4 hours of administration (Fig. 5, E and F). Notably, strong fluorescence signals of INS released from T@I@U were observed in the liver, indicating that INS might initially circulate through the portal veins to the liver, consistent with the endogenous INS secretion behavior. It can be seen that free INS did not show any fluorescence signal in major organs, owing to the rapid degradation of proteins in the GI tract under extreme pH conditions and protease environment. Despite the fact that a small amount of INS from I@U in the liver was observed, the fluorescence signal of INS was fragile compared with the Tf-coated nMOFs group, representing the inefficient absorption of INS through the intestine without Tf decoration.

To further verify the potential pathway for the T@I@U to cross the epithelial layer, the intestine epithelial tissues were sectioned and processed for confocal imaging after 2 hours of administration (Fig. 5G). The fluorescence signal located inside the epithelial cells confirmed that INS from T@I@U was transported into the intestinal villi successfully, while barely any fluorescence had been found in the free INS and I@U group. The above results indicated that only the Tf-coated acid-resistant MOFs could significantly improve the permeability of INS in the intestine and realize INS transportation orally.

In vivo pharmacodynamics and pharmacokinetics studies

To investigate the hypoglycemic response and pharmacokinetics parameters of the INS-loaded nMOFs, we administered the INS-loaded nMOFs (20 IU kg^{-1}) and free INS (20 IU kg^{-1}) to alloxan-induced diabetic rats/mice by gavage and subcutaneously injected the free INS (5 IU kg^{-1}) to alloxan-induced diabetic rats. The blood glucose and serum INS concentrations were monitored using a glucometer and bovine INS ELISA (enzyme-linked immunosorbent assay) assay, respectively. As shown in Fig. 5 (H and I), oral administration of free INS and I@U failed to reduce the blood glucose levels (BGLs), while free INS (subcutaneous) group and T@I@U intragastric administration group generated a strong hypoglycemic response in contrast. The free INS (subcutaneous) group caused a sharp decrease in BGLs to about 28% of the initial level at 2 hours, and the hypoglycemic effect subsequently wore off 4 hours later. Compared with the free INS (subcutaneous) group, the T@I@U quickly reduced BGL to around 30% of the initial level in the first 2 hours and led to a prolonged reduction in BGL during 8 hours. On the basis of the glucose-decreasing profile, the relative pharmacological activity of T@I@U was calculated to be 31.9%. The corresponding serum INS profiles of rats treated with different formulations were depicted as the area under the curve ($AUC_{0\text{-}12\ h}$) in Fig. 5J, representing a consistent result with pharmacodynamics. The maximum serum INS level of free INS (subcutaneous) appeared within 1 hour and returned to a minimum in only 4 hours. Compared with the free INS group, the T@I@U group could maintain a relatively high and stable serum INS level for up to 10 hours. The above experimental results indicated that Tf-coated nMOFs could prolong the INS efficacy in vivo and reduce the transient hypoglycemia side effects caused by the free INS injection. The pharmacokinetic parameters calculated from peripheral serum INS are shown in table S2. The AUC of T@I@U was 120.7 mIU × hour/liter with a relative bioavailability of 29.6%, which was 42.3- and 26.9-fold higher than that of oral INS solution (0.7%) and the I@U group (1.1%), respectively.

DISCUSSION

In conclusion, we have successfully fabricated a highly effective oral INS delivery system based on Tf-coated acid-resistant nMOFs (T@I@U) through a simple, low-cost, and easy scale-up process. The highly porous nMOFs demonstrated high protein drug LC (up to 33 wt %) unattainable by most INS nanocarriers. By constructing T@I@U, INS was well protected by the nMOFs and Tf under the harsh environment in the GI tract and overcame the gastric acid

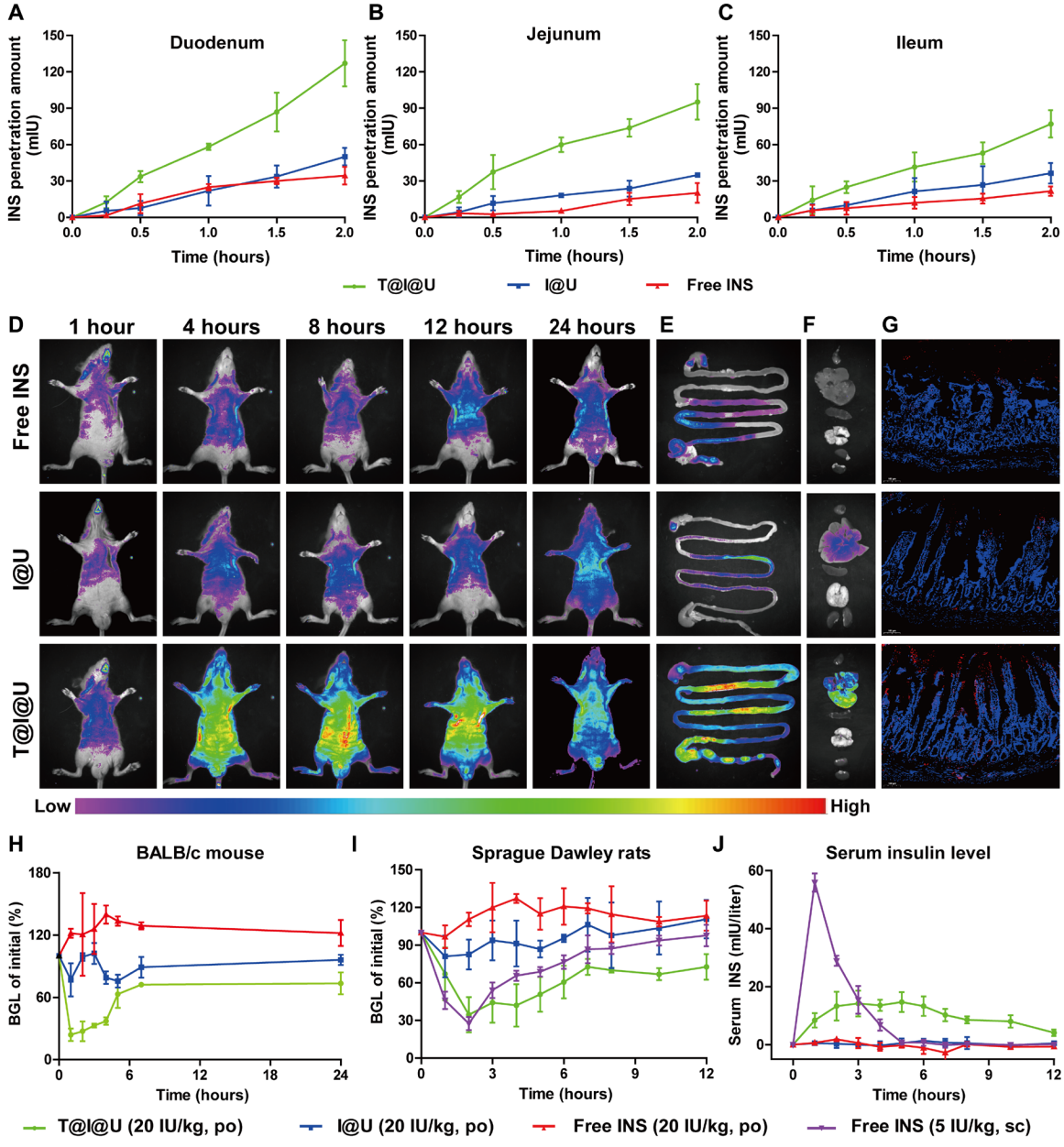

Fig. 5. Verification of the enhanced absorption of INS in animals. Ex vivo permeation studies of INS from different formulations across the different intestinal segments [(**A**) duodenum, (**B**) jejunum, and (**C**) ileum] ($n = 3$ biologically independent samples, means ± SD). (**D**) Fluorescence distribution and intensity of the RITC-INS in vivo after the oral INS administration from different formulations at different time points. Ex vivo fluorescence images of the intestine (**E**) and images of heart, liver, spleen, lung, and kidney (from top to bottom) (**F**) of the mice after the oral INS administration for 4 hours. (**G**) CLSM images of sectioned intestine tissues of rats after oral administration of different INS formulations for 2 hours. BGLs of initial versus time profiles of the diabetic BALB/C mouse (**H**) and Sprague-Dawley rats (**I**) following the oral administration of different INS formulations ($n = 6$ biologically independent animals, means ± SD). (**J**) The serum INS concentration (bioavailability) for the T@I@U, I@U, and free INS on diabetic rats through oral gavage ($n = 3$ biologically independent animals, means ± SD). po, per os; sc, subcutaneously.

barrier, while it exhibited sustained and controlled release kinetics under physiological conditions. Meanwhile, the easy modification feature of nMOFs allowed Tf to be facilely installed on the well-defined surface to alter the nMOFs' penetration behaviors, providing synthetic advantages over those Tf-conjugated delivery nanosystems. The cellular experiments indicated that T@I@U first achieved effective apical endocytosis via the Tf-mediated uptake pathway, subsequently realized rapid lysosome escape through the unique membrane switching effect, and released from the cell monolayer eventually to overcome the basolateral membrane barrier. More significantly, we verified the effectiveness of T@I@U by small-animal research in which T@I@U quickly reduced BGL to around 30% of the initial level and prolonged the INS efficacy to 10 hours, bringing about a high oral bioavailability of 29.6%, which is about four times of that reported in Tf-decorated polymeric NPs (*29*). Besides, no tissue damage and abnormality of animals were observed in the

long-term experiment, indicating the good biocompatibility of such an oral delivery nanosystem. On the basis of the above performance, we believe that Tf-coated acid-resistant nMOFs are general oral protein delivery vehicles that could conquer various physiological obstacles in the GI tract. This nanosystem combines the advantages of efficient protein loading and protection, good intestinal permeability, controllable protein release, and a simple formulation strategy, holding great promise for expanding the utility of protein-based oral therapies. Nevertheless, the effectiveness of this nanosystem still needs to be further investigated in large animal species, in which the gastric emptying rate is slower and may aggravate the degradation of the nanosystem and the installed therapeutic or targeting protein. Furthermore, such a simple and effective MOF-based nanosystem could be expandable to integrate carefully selected therapeutic proteins with coated targeting proteins to create diverse functional nanosystems, providing the possibility to meet a wide range of biomedical applications in the future.

MATERIALS AND METHODS

Materials

All standard synthesis reagents were purchased from commercial suppliers and used without any further purification. $ZrOCl_2{\cdot}8H_2O$, 2,5-dibromobenzenamine, 4-(methoxycarbonyl) phenylboronic acid, CsF, $Pd(PPh_3)_4$, RITC, and FITC were obtained from Energy Chemical. NaOH and CH_3COOH were purchased from Sinopharm Chemical Reagent. INS, Tf, 4′,6-diamidino-2-phenylindole (DAPI), lysosome tracker, and the BCA kit were obtained from Bio-sharp (Hefei, China). MTT and Dulbecco's modified Eagle's medium (DMEM) were purchased from Wuhan Kerui Biotechnology Co. Ltd. The bovine INS ELISA kit was obtained from Jiangsu Meimian Industrial Co. Ltd.

Preparation of UiO-68-NH_2, I@U, and T@I@U

Amino-triphenyl dicarboxylic acid (amino-TPDC) was synthesized according to the modifying methods as previously reported (*47*). UiO-68-NH_2 was prepared through the solvothermal method. In brief, amino-TPDC (8.3 mg, 0.025 mmol) and $ZrOCl_2{\cdot}8H_2O$ (10.5 mg, 0.032 mmol) were dissolved in 2 ml of DMF. The mixture was sonicated for 5 min until it was clear and transparent. Acetic acid (40 μl) was added to the mixture and then heated at 90°C for 6 hours. The purified UiO-68-NH_2 was obtained by centrifuging the mixture and washing it three times with DMF. The solvent was exchanged into ddH_2O by centrifugation three times; 100 μl of the solution was dried to powder and weighed for quantification.

For the preparation of I@U, 200 μl of INS solution (20 mg/ml, dissolved in dilute HCl, pH 2.0) was added dropwise to 4 ml of freshly synthesized UiO-68-NH_2 dispersion (0.25 mg/ml in ddH_2O) and stirred for 12 hours at room temperature to obtain I@U. Subsequently, 40 μl of Tf solution (5 mg/ml in ddH_2O) was added to the above solution and was continuously stirred for 12 hours to obtain T@I@U. Different feeding ratios (INS: UiO-68-NH_2 = 1:1, 2:1, 4:1, 6:1; Tf: UiO-68-NH_2 = 1:10, 2:10, 5:10, 10:10) were separately investigated to optimize parameters of the INS loading and Tf coating. The highest INS LC was achieved with a feeding ratio of INS: UiO-68-NH_2 = 4:1. For the Tf coating, the optimal feeding ratio is determined to be Tf: UiO-68-NH_2 = 2:10. The higher feeding ratio beyond 2:10 resulted in a small percentage of aggregated T@I@U NPs observed by transmission electron microscopy (TEM). To remove the free INS and Tf attached to the surface of MOF NPs, the supernatant was discarded, and the solid samples were washed with ddH_2O and then collected by centrifuge. INS loading content was measured by the BCA kit, and TGA. INS loading content was calculated by:

Loading content = (total weight of drug-weight of drug in supernatant)/weight of drug-loaded NPs × 100%.

Characterization

Zeta potential and hydrodynamic size of UiO-68-NH_2, I@U, and T@I@U were measured by Malvern Zetasizer Nano series ZS-90. The TEM tests were performed by HITACHI H-7000FA TEM to evaluate the morphology of the samples. The EDS elemental mapping analysis was performed by FEI Talos F200X. PXRD was carried out with a Rigaku MiniFlex 600 x-ray diffractometer under Cu Kα radiation (parameter, 600 W). The UV-vis spectroscopy was measured by a UV-vis spectrophotometer (UV-2600, Shimadzu, Japan). The fluorescence signal of the nanosystems was detected by a fluorescence spectrophotometer (RF-6000, Shimadzu, Japan). The TGA was observed by TGA 50. CLSM images were collected by Carl Zeiss NOL-LSM 710.

In vitro stability

To test the stability of UiO-68-NH_2–based nanosystems, the different formulations were respectively dispersed in SGF, PBS, and DMEM cell medium containing 10% fetal bovine serum (FBS), and the size at various time points were measured by dynamic light scattering (DLS). To determine whether UiO-68-NH_2 could protect INS from digestive enzymes, the NPs were incubated in simulated intestinal fluid containing trypsin (1 mg/ml) at 37°C. Aliquots (100 μl) at specific time intervals were taken out and 200 μl of dimethyl sulfoxide (DMSO) containing 0.1% trifluoroacetic acid was added to stop the enzymatic reaction. The concentration of INS was determined with the ELISA kit in all the following experiments.

Release kinetics

To test the release behaviors of I@U and T@I@U, samples were placed in dialysis bags [molecular weight cutoff (MWCO) = 10 kDa] and dispersed in ddH_2O, FaSSGF, FaSSIF (without phosphate), and PBS at 37°C for 24 hours. In addition, we simulated the status of orally taken I@U and T@I@U by dialyzing the NPs against FaSSGF for 2 hours, followed by FaSSIF for another 2 hours and PBS (pH 7.4) for an additional 8 hours. At different time points, 100 μl of buffer was taken, and an equal volume of fresh buffer was added to ensure a constant volume. The content of INS was determined using the BCA kit.

To study the bioactivity of INS after the preparation and drug release process, I@U and T@I@U were immersed in PBS for 24 hours at 37°C and isolated by ultracentrifugation. The content of the released INS was determined using the BCA kit. Then, the released INS (5 IU/kg) or free INS (5 IU/kg) was administered to the overnight-fasting Sprague-Dawley rats by subcutaneous injection.

Hemolysis test

The mouse blood samples were mixed with different concentrations of T@I@U in physiological saline solution (0, 0.125, 0.25, 0.5, 0.75, and 1 mg/ml) and incubated at 37°C for 4 hours. The erythrocytes

were mixed with H_2O in the positive group and saline in the negative group, respectively. After centrifugation, the UV absorption value of the supernatant at 540 nm was measured, and the hemolysis rate of the sample was calculated according to the formula

$$\text{Hemolysis} = (A_{samples} - A_{negative})/(A_{positive} - A_{negative}) \times 100\%$$

Cell culture

The human colon adenocarcinoma cell line (Caco-2) was purchased from the China Type Culture Collection. Caco-2 cells were cultured in a DMEM medium containing 20% FBS and 1% penicillin-streptomycin and placed in a 37°C, 5% CO_2 cell incubator.

Cell cytotoxicity study in vitro

Different cell lines at the density of 1×10^4 cells per well were cultured in 96-well plates separately. A series of doses of UiO-68-NH_2, I@U, and T@I@U (0, 31.25, 62.5, 125, 250, and 500 μg/ml) in the culture medium was applied to the cells for 24 hours at 37°C with 5% CO_2, and five samples were taken in parallel. The medium was discarded, and the cells were exposed to freshly prepared MTT solution (5 mg/ml) for another 4 hours. Afterward, DMSO (100 μl) was added to wells. The optical density was monitored at 490 nm using a microplate reader.

Live/dead cell viability assay

Caco-2 cells were seeded in 12-well plates and cultured for 3 days. The cells were treated with DMEM medium containing different samples for 24 hours, and the live/dead cells were stained with calcein AM and propidium iodide. The images were taken by an inverted fluorescence microscope.

Cellular internalization studies in vitro

To visualize the uptake of UiO-68-NH_2, I@U, and T@I@U, Caco-2 cells were cultured in 12-well plates with slides for 3 days and incubated with either free RITC-INS, RITC-INS@U, or T@RITC-INS@U at 37°C for different time intervals. Subsequently, the cells were fixed with 4% paraformaldehyde and stained with DAPI for 20 min. After rinsing the slides with PBS, the location of NPs in cells was observed by CLSM (LSM 800, Zeiss, Germany). The intensity of fluorescence was also measured by flow cytometry.

To further evaluate the role of Tf in the uptake trial, Caco-2 cells were incubated with double-labeled T@I@U. In addition, the cellular uptake of T@I@U was studied with prior incubation with Tf. After incubation with different formulations for 2 hours at 37°C, the amounts of RITC-INS were determined using CLSM.

The colocalization of nMOFs and lysosomes was characterized. In brief, T@RITC-INS@U were added to the cells and incubated at 37°C for various time intervals (15, 30, 60, 120, and 240 min). Subsequently, Caco-2 cells were stained with LysoTracker Green for 30 min. The CLSM was used to analyze the colocalization of the samples and lysosomes.

The deep penetration of T@I@U was studied as the literature reported. Caco-2 cells on coverslips (i) were cultured in a medium that contained different INS formulations for 4 hours. Then, coverslip (i) was put into fresh culture medium and fresh cells on the coverslip (ii) for 12 hours. The above step was repeated to obtain the coverslip (iii). The coverslips (i, ii, and iii) were visualized by CLSM separately.

In vitro transepithelial transport

The Caco-2 cells were seeded into a Transwell insert and cultured for 3 weeks until the cell monolayer membrane was formed (the TEER values reached above 500 ohm × cm^2). Free INS, I@U, and T@I@U in the medium were added to the apical side. Samples were taken out from the basolateral side at 0, 0.083, 0.25, 0.5, 1, 1.5, and 2 hours, and the medium was always supplemented to keep the volume consistent. During the process, the TEER values were constantly measured to determine the integrity of tight junctions. The INS contents were measured using the bovine INS ELISA kit. The Papp values of INS from the different treatments were calculated as reported.

Animal models

Male Sprague-Dawley rats (180 to 200 g) and BALB/c mice (18 to 20 g) were provided by Beijing Vital River Laboratory Animal Technology Co. Ltd. All the animal studies were conducted following the Chinese Regulations for the Administration of Affairs Concerning Experimental Animals and performed in compliance with the guidelines of the Institutional Animal Care and Use Committee of Wuhan University.

The isolated intestine penetration test

The intestinal penetration experiment in vitro was carried out according to the method reported in the literature. The Sprague-Dawley rats were fasted overnight and then euthanized. A total of 5 cm of duodenum, jejunum, and ileum with both ends ligated were taken out, and then 200 μl of free INS, I@U, and T@I@U (10 IU/ml) was injected into the intestinal lumen. The intestine was then incubated in 5 ml of PBS buffer at 37°C with gentle stirring. The samples were collected according to the above method, and the amount of INS released was again quantified by ELISA kit.

In vivo fluorescence imaging

RITC-INS, RITC-INS@U, and T@RITC-INS@U were orally administered to the overnight-fasted mice. The fluorescence images of mice were captured at different time points using the SI Imaging Amix imaging system to evaluate the metabolic process of INS preparations. Another group of mice was euthanized after 4 hours of treatment. The images of organs and intestines were also obtained. Different formulations were orally administered to the overnight-fasted rats for 4 hours. Then, the rats were euthanized, and the intestine loops were excised and frozen in Tissue-Tek optimum cutting temperature compound (OCT compound) with liquid nitrogen. Cross intestine sections were obtained using a freezing microtome blade, and then, the intestine sections were stained with DAPI for 10 min and visualized by CLSM.

INS bioactivity in vivo

In vivo studies were performed in alloxan-induced diabetic animals ($n = 6$ per group). The rats and mice were induced to type 1 diabetes by alloxan injections. The animals were regarded as diabetic if their fasting BGL were higher than 11 mmol/liter in 1 week after injection.

The rats and mice fasted overnight before experiments and then administered different samples by gavage. The hypoglycemic effect was tested following the oral administration of I@U and T@I@U (20 IU/kg). As control groups, one group of rats were administered free INS (20 IU/kg) by oral gavage, and the other group was administered free INS (5 IU/kg) by subcutaneous injection. Blood samples

were collected from the orbital venous plexus and analyzed using a blood glucose meter, expressed as the percentage of baseline serum glucose level (0 hours) at different periods. The INS contents in blood samples were measured using the bovine INS ELISA kit. The 0-hour INS content was subtracted from the INS measured at different time intervals and plotted.

Histologic examination

Mice received oral gavage with free INS, I@U, and T@I@U twice a day for seven consecutive days. The mice were euthanized, and their organs and intestines were put in 4% (w/v) formalin. Then, the organs were embedded in paraffin, and the tissue was cut into slices, both of which were later stained with hematoxylin and eosin for microscopic examination.

Statistical analysis

Statistical significance was determined by a two-tailed Student's *t* test. The differences were considered significant for P values * < 0.05, ***< 0.001. Unless otherwise noted, all parallel experiments are conducted in three groups ($n = 3$). Error bars used in this work were SD.

SUPPLEMENTARY MATERIALS

Supplementary material for this article is available at https://science.org/doi/10.1126/sciadv.abm4677

View/request a protocol for this paper from *Bio-protocol*.

REFERENCES AND NOTES

1. IDF congress 2019: Shaping the future of diabetes. *Diabetes Res. Clin. Pract.* **158**, 107954 (2019).
2. L. A. DiMeglio, C. Evans-Molina, R. A. Oram, Type 1 diabetes. *Lancet* **391**, 2449–2462 (2018).
3. S. Chatterjee, K. Khunti, M. J. Davies, Type 2 diabetes. *Lancet* **389**, 2239–2251 (2017).
4. H. Malhaire, J.-C. Gimel, E. Roger, J.-P. Benoit, F. Lagarce, How to design the surface of peptide-loaded nanoparticles for efficient oral bioavailability? *Adv. Drug Deliver. Rev.* **106**, 320–336 (2016).
5. R. Mo, T. Jiang, J. Di, W. Tai, Z. Gu, Emerging micro- and nanotechnology based synthetic approaches for insulin delivery. *Chem. Soc. Rev.* **43**, 3595–3629 (2014).
6. American Diabetes Association, Standards of medical care in diabetes—2016 Abridged for primary care providers. *Clin. Diabetes* **34**, 3–21 (2016).
7. V. Sinha, A. Singh, R. V. Kumar, S. Singh, R. Kumria, J. Bhinge, Oral colon-specific drug delivery of protein and peptide drugs. *Crit. Rev. Ther. Drug Carrier Syst.* **24**, 63–92 (2007).
8. H. Iyer, A. Khedkar, M. Verma, Oral insulin - a review of current status. *Diabetes Obes. Metab.* **12**, 179–185 (2010).
9. X. Qi, Y. Yuan, J. Zhang, J. W. M. Bulte, W. Dong, Oral administration of salecan-based hydrogels for controlled insulin delivery. *J. Agric. Food Chem.* **66**, 10479–10489 (2018).
10. A. M. Wagner, M. P. Gran, N. A. Peppas, Designing the new generation of intelligent biocompatible carriers for protein and peptide delivery. *Acta Pharm. Sin. B* **8**, 147–164 (2018).
11. Y. Xiao, Z. Tang, J. Wang, C. Liu, N. Kong, O. C. Farokhzad, W. Tao, Oral insulin delivery platforms: Strategies to address the biological barriers. *Angew. Chem. Int. Ed. Engl.* **59**, 19787–19795 (2020).
12. D. J. Drucker, Advances in oral peptide therapeutics. *Nat. Rev. Drug Discov.* **19**, 277–289 (2020).
13. S. Chopra, N. Bertrand, J.-M. Lin, A. Wang, O. C. Farokhzad, R. Karnik, Design of insulin-loaded nanoparticles enabled by multistep control of nanoprecipitation and zinc chelation. *ACS Appl. Mater. Interfaces* **9**, 11440–11450 (2017).
14. E. Juere, R. Caillard, D. Marko, G. Del Favero, F. Kleitz, Smart protein-based formulation of dendritic mesoporous silica nanoparticles: Toward oral delivery of insulin. *Chemistry* **26**, 5195–5199 (2020).
15. A. Wang, T. Yang, W. Fan, Y. Yang, Q. Zhu, S. Guo, C. Zhu, Y. Yuan, T. Zhang, Y. Gan, Protein corona liposomes achieve efficient oral insulin delivery by overcoming mucus and epithelial barriers. *Adv. Healthc. Mater.* **8**, e1801123 (2019).
16. J. P. Martins, R. D'Auria, D. Liu, F. Fontana, M. P. A. Ferreira, A. Correia, M. Kemell, K. Moslova, E. Mäkilä, J. Salonen, L. Casettari, J. Hirvonen, B. Sarmento, H. A. Santos, Engineered multifunctional albumin-decorated porous silicon nanoparticles for FcRn translocation of insulin. *Small* **14**, e1800462 (2018).
17. W. Shan, X. Zhu, M. Liu, L. Li, J. Zhong, W. Sun, Z. Zhang, Y. Huang, Overcoming the diffusion barrier of mucus and absorption barrier of epithelium by self-assembled nanoparticles for oral delivery of insulin. *ACS Nano* **9**, 2345–2356 (2015).
18. M. A. Mumuni, F. C. Kenechukwu, K. C. Ofokansi, A. A. Attama, D. D. Diaz, Insulin-loaded mucoadhesive nanoparticles based on mucin-chitosan complexes for oral delivery and diabetes treatment. *Carbohydr. Polym.* **229**, 115506 (2020).
19. Y. Zhou, L. Liu, Y. Cao, S. Yu, C. He, X. Chen, A nanocomposite vehicle based on metal-organic framework nanoparticle incorporated biodegradable microspheres for enhanced oral insulin delivery. *ACS Appl. Mater. Interfaces* **12**, 22581–22592 (2020).
20. S. Seyam, N. A. Nordin, M. Alfatama, Recent progress of chitosan and chitosan derivatives-based nanoparticles: Pharmaceutical perspectives of oral insulin delivery. *Pharmaceuticals (Basel)* **13**, 307 (2020).
21. E. J. B. Nielsen, S. Yoshida, N. Kamei, R. Iwamae, E.-S. Khafagy, J. Olsen, U. L. Rahbek, B. L. Pedersen, K. Takayama, M. Takeda-Morishita, In vivo proof of concept of oral insulin delivery based on a co-administration strategy with the cell-penetrating peptide penetratin. *J. Control. Release* **189**, 19–24 (2014).
22. Y. Zhou, Z. Chen, D. Zhao, D. Li, C. He, X. Chen, A pH-triggered self-unpacking capsule containing zwitterionic hydrogel-coated MOF nanoparticles for efficient oral exendin-4 delivery. *Adv. Mater.* **33**, e2102044 (2021).
23. A. Lerner, T. Matthias, Changes in intestinal tight junction permeability associated with industrial food additives explain the rising incidence of autoimmune disease. *Autoimmun. Rev.* **14**, 479–489 (2015).
24. X. Han, Y. Lu, J. Xie, E. Zhang, H. Zhu, H. Du, K. Wang, B. Song, C. Yang, Y. Shi, Z. Cao, Zwitterionic micelles efficiently deliver oral insulin without opening tight junctions. *Nat. Nanotechnol.* **15**, 605–614 (2020).
25. M. A. Odenwald, J. R. Turner, The intestinal epithelial barrier: A therapeutic target? *Nat. Rev. Gastroenterol. Hepatol.* **14**, 9–21 (2017).
26. J. T. Sockolosky, F. C. Szoka, The neonatal Fc receptor, FcRn, as a target for drug delivery and therapy. *Adv. Drug Deliver. Rev.* **91**, 109–124 (2015).
27. E. M. Pridgen, F. Alexis, T. T. Kuo, E. Levy-Nissenbaum, R. Karnik, R. S. Blumberg, R. Langer, O. C. Farokhzad, Transepithelial transport of Fc-targeted nanoparticles by the neonatal Fc receptor for oral delivery. *Sci. Transl. Med.* **5**, 213ra167 (2013).
28. D. Banerjee, P. R. Flanagan, J. Cluett, L. S. Valberg, Transferrin receptors in the human gastrointestinal tract. Relationship to body iron stores. *Gastroenterology* **91**, 861–869 (1986).
29. X. Zhu, J. Wu, W. Shan, W. Tao, L. Zhao, J.-M. Lim, M. D'Ortenzio, R. Karnik, Y. Huang, J. Shi, O. C. Farokhzad, Polymeric nanoparticles amenable to simultaneous installation of exterior targeting and interior therapeutic proteins. *Angew. Chem. Int. Ed. Engl.* **55**, 3309–3312 (2016).
30. D. T. Wiley, P. Webster, A. Gale, M. E. Davis, Transcytosis and brain uptake of transferrin-containing nanoparticles by tuning avidity to transferrin receptor. *Proc. Natl. Acad. Sci. U.S.A.* **110**, 8662–8667 (2013).
31. A. Dautry-Varsat, A. Ciechanover, H. F. Lodish, pH and the recycling of transferrin during receptor-mediated endocytosis. *Proc. Natl. Acad. Sci. U.S.A.* **80**, 2258–2262 (1983).
32. N. J. Kavimandan, E. Losi, N. A. Peppas, Novel delivery system based on complexation hydrogels as delivery vehicles for insulin-transferrin conjugates. *Biomaterials* **27**, 3846–3854 (2006).
33. N. J. Kavimandan, E. Losi, J. J. Wilson, J. S. Brodbelt, N. A. Peppas, Synthesis and characterization of insulin-transferrin conjugates. *Bioconjug. Chem.* **17**, 1376–1384 (2006).
34. C. M. Lawrence, S. Ray, M. Babyonyshev, R. Galluser, D. W. Borhani, S. C. Harrison, Crystal structure of the ectodomain of human transferrin receptor. *Science* **286**, 779–782 (1999).
35. W. Du, Y. Fan, N. Zheng, B. He, L. Yuan, H. Zhang, X. Wang, J. Wang, X. Zhang, Q. Zhang, Transferrin receptor specific nanocarriers conjugated with functional 7peptide for oral drug delivery. *Biomaterials* **34**, 794–806 (2013).
36. W. C. Duckworth, Insulin degradation: Mechanisms, products, and significance. *Endocr. Rev.* **9**, 319–345 (1988).
37. S. Wang, C. M. McGuirk, A. d'Aquino, J. A. Mason, C. A. Mirkin, Metal-organic framework nanoparticles. *Adv. Mater.* **30**, e1800202 (2018).
38. S. Wang, Y. Chen, S. Wang, P. Li, C. A. Mirkin, O. K. Farha, DNA-functionalized metal-organic framework nanoparticles for intracellular delivery of proteins. *J. Am. Chem. Soc.* **141**, 2215–2219 (2019).
39. T. Simon-Yarza, A. Mielcarek, P. Couvreur, C. Serre, Nanoparticles of metal-organic frameworks: On the road to in vivo efficacy in biomedicine. *Adv. Mater.* **30**, e1707365 (2018).
40. W. Liang, P. Wied, F. Carraro, C. J. Sumby, B. Nidetzky, C. K. Tsung, P. Falcaro, C. J. Doonan, Metal-organic framework-based enzyme biocomposites. *Chem. Rev.* **121**, 1077–1129 (2021).
41. A. P. Katsoulidis, D. Antypov, G. F. S. Whitehead, E. J. Carrington, D. J. Adams, N. G. Berry, G. R. Darling, M. S. Dyer, M. J. Rosseinsky, Chemical control of structure and guest uptake by a conformationally mobile porous material. *Nature* **565**, 213–217 (2019).
42. M.-X. Wu, Y.-W. Yang, Metal-organic framework (MOF)-based drug/cargo delivery and cancer therapy. *Adv. Mater.* **29**, e1606134 (2017).
43. Q. Chen, M. Xu, W. Zheng, T. Xu, H. Deng, J. Liu, Se/Ru-decorated porous metal-organic framework nanoparticles for the delivery of pooled siRNAs to reversing multidrug

resistance in taxol-resistant breast cancer cells. *ACS Appl. Mater. Interfaces* **9**, 6712–6724 (2017).
44. H. Wang, Y. Chen, H. Wang, X. Liu, X. Zhou, F. Wang, DNAzyme-loaded metal-organic frameworks (MOFs) for self-sufficient gene therapy. *Angew. Chem. Int. Ed. Engl.* **58**, 7380–7384 (2019).
45. G. Collet, T. Lathion, C. Besnard, C. Piguet, S. Petoud, On-demand degradation of metal-organic framework based on photocleavable dianthracene-based ligand. *J. Am. Chem. Soc.* **140**, 10820–10828 (2018).
46. Y. Chen, P. Li, J. A. Modica, R. J. Drout, O. K. Farha, Acid-resistant mesoporous metal-organic framework toward oral insulin delivery: Protein encapsulation, protection, and release. *J. Am. Chem. Soc.* **140**, 5678–5681 (2018).
47. Z. Li, X. Qiao, G. He, X. Sun, D. Feng, L. Hu, H. Xu, H.-B. Xu, S. Ma, J. Tian, Core-satellite metal-organic framework@upconversion nanoparticle superstructures via electrostatic self-assembly for efficient photodynamic theranostics. *Nano Res.* **13**, 3377–3386 (2020).
48. A. Schaate, P. Roy, A. Godt, J. Lippke, F. Waltz, M. Wiebcke, P. Behrens, Modulated synthesis of Zr-based metal-organic frameworks: From nano to single crystals. *Chemistry* **17**, 6643–6651 (2011).
49. P. S. Oates, E. H. Morgan, Ferritin gene expression and transferrin receptor activity in intestine of rats with varying iron stores. *Am. J. Physiol.* **273**, G636–G646 (1997).
50. W. Fan, D. Xia, Q. Zhu, X. Li, S. He, C. Zhu, S. Guo, L. Hovgaard, M. Yang, Y. Gan, Functional nanoparticles exploit the bile acid pathway to overcome multiple barriers of the intestinal epithelium for oral insulin delivery. *Biomaterials* **151**, 13–23 (2018).
51. A. Wang, W. Fan, T. Yang, S. He, Y. Yang, M. Yu, L. Fan, Q. Zhu, S. Guo, C. Zhu, Y. Gan, Liver-target and glucose-responsive polymersomes toward mimicking endogenous insulin secretion with improved hepatic glucose utilization. *Adv. Funct. Mater.* **30**, e1910168 (2020).
52. Q. Zhou, S. Shao, J. Wang, C. Xu, J. Xiang, Y. Piao, Z. Zhou, Q. Yu, J. Tang, X. Liu, Z. Gan, R. Mo, Z. Gu, Y. Shen, Enzyme-activatable polymer-drug conjugate augments tumour penetration and treatment efficacy. *Nat. Nanotechnol.* **14**, 799–809 (2019).

Acknowledgments
Funding: This work was financially supported by the following funding: National Natural Science Foundation of China no. NSFC 21601140 (J.T.), National Natural Science Foundation of China no. NSFC 21871214 (J.T.), Fundamental Research Funds for the Central Universities 2042017kf0186 (J.T.), and Robert A Welch Foundation (B-0027) (S.M.). **Author contributions:** Conceptualization: J.-J.Z., J.T., and S.M. Methodology: J.-J.Z., G.W., Y.Y., and S.L. Investigation: J.-J.Z. and C.X. Visualization: J.-J.Z. and L.H. Supervision: J.T. Writing—original draft: J.-J.Z., J.T., and S.M. **Competing interests:** The authors declare that they have no competing interests. **Data and materials availability:** All data needed to evaluate the conclusions in the paper are present in the paper and/or the Supplementary Materials.

Submitted 20 September 2021
Accepted 29 December 2021
Published 23 February 2022
10.1126/sciadv.abm4677